This paper is published as part of a *Nanoscale* themed issue on doped nanostructures

Guest Editor: Stephen Pearton

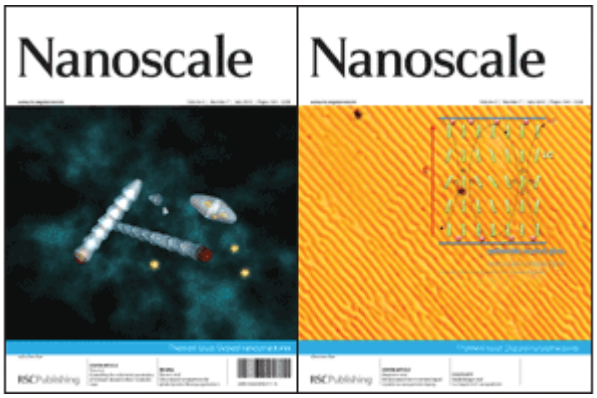

Editorial

Doped nanostructures
Stephen Pearton, *Nanoscale*, 2010
DOI: 10.1039/c005273f

Review Articles

Impacts of doping on thermal and thermoelectric properties of nanomaterials
Gang Zhang and Baowen Li, *Nanoscale*, 2010
DOI: 10.1039/c0nr00095g

Effect of N/B doping on the electronic and field emission properties for carbon nanotubes, carbon nanocones, and graphene nanoribbons
Shan-Sheng Yu and Wei-Tao Zheng, *Nanoscale*, 2010
DOI: 10.1039/c0nr00002g

Silica-based nanoparticles for photodynamic therapy applications
Pierre Couleaud, Vincent Morosini, Céline Frochot, Sébastien Richeter, Laurence Raehm and Jean-Olivier Durand, *Nanoscale*, 2010
DOI: 10.1039/c0nr00096e

Mini Review

Co-Doped ZnO nanoparticles: Minireview
Igor Djerdj, Zvonko Jagli?i?, Denis Ar?on and Markus Niederberger, *Nanoscale*, 2010
DOI: 10.1039/c0nr00148a

Communications

Controlling the volumetric parameters of nitrogen-doped carbon nanotube cups
Brett L. Allen, Matthew B. Keddie and Alexander Star, *Nanoscale*, 2010
DOI: 10.1039/c0nr00043d

Visible light induced photobleaching of methylene blue over melamine-doped TiO_2 nanocatalyst
Jurate Virkutyte, Babita Baruwati and Rajender S. Varma, *Nanoscale*, 2010
DOI: 10.1039/c0nr00089b

Selective detection of trace amount of Cu^{2+} using semiconductor nanoparticles in photoelectrochemical analysis
Guang-Li Wang, Jing-Juan Xu and Hong-Yuan Chen, *Nanoscale*, 2010
DOI: 10.1039/c0nr00084a

Flower-like TiO_2 nanosructures with exposed {001} facets: Facile synthesis and enhanced photocatalysis
Min Liu, Lingyu Piao, Weiming Lu, Siting Ju, Lei Zhao, Chunlan Zhou, Hailing Li and Wenjing Wang, *Nanoscale*, 2010
DOI: 10.1039/c0nr00050g

Papers

Electroconvection in nematic liquid crystals *via* nanoparticle doping
Martin Urbanski, Brandy Kinkead, Hao Qi, Torsten Hegmann and Heinz-S. Kitzerow, *Nanoscale*, 2010
DOI: 10.1039/c0nr00139b

Superhydrophilicity-assisted preparation of transparent and visible light activated N-doped titania film
Qing Chi Xu, Diana V. Wellia, Rose Amal, Dai Wei Liao, Say Chye Joachim Loo and Timothy Thatt Yang Tan, *Nanoscale*, 2010
DOI: 10.1039/c0nr00105h

The influence of doping on the device characteristics of $In_{0.5}Ga_{0.5}As/GaAs/Al_{0.2}Ga_{0.8}As$ quantum dots-in-a-well infrared photodetectors
G. Jolley, L. Fu, H. H. Tan and C. Jagadish, *Nanoscale*, 2010
DOI: 10.1039/c0nr00128g

Study of concentration-dependent cobalt ion doping of TiO_2 and $TiO_{2-x}N_x$ at the nanoscale
James L. Gole, Sharka M. Prokes, O. J. Glembocki, Junwei Wang, Xiaofeng Qiu and Clemens Burda, *Nanoscale*, 2010
DOI: 10.1039/c0nr00125b

Multifunctional nanocomposites of superparamagnetic (Fe_3O_4) and NIR-responsive rare earth-doped up-conversion fluorescent ($NaYF_4$: Yb,Er) nanoparticles and their applications in biolabeling and fluorescent imaging of cancer cells
Congcong Mi, Jingpu Zhang, Huanyu Gao, Xianlong Wu, Meng Wang, Yingfan Wu, Yueqin Di, Zhangrun Xu, Chuanbin Mao and Shukun Xu, *Nanoscale*, 2010
DOI: 10.1039/c0nr00102c

Effect of doping on the morphology and multiferroic properties of $BiFeO_3$ nanorods
Dimple P. Dutta, O. D. Jayakumar, A. K. Tyagi, K. G. Girija, C. G. S. Pillai and G. Sharma, *Nanoscale*, 2010
DOI: 10.1039/c0nr00100g

Effect of substrate temperature on implantation doping of Co in CdS nanocrystalline thin films
S. Chandramohan, A. Kanjilal, S. N. Sarangi, S. Majumder, R. Sathyamoorthy, C.-H. Hong and T. Som, *Nanoscale*, 2010
DOI: 10.1039/c0nr00123f

Modification of neodymium-doped ZnO hybrid nanoparticles under mild hydrothermal conditions
Behzad Shahmoradi, K. Soga, S. Ananda, R. Somashekar and K. Byrappa, *Nanoscale*, 2010
DOI: 10.1039/c0nr00069h

***Ex situ* vapor phase boron doping of silicon nanowires using BBr_3**
Gregory S. Doerk, Gabriella Lestari, Fang Liu, Carlo Carraro and Roya Maboudian, *Nanoscale*, 2010
DOI: 10.1039/c0nr00127a

Change in conformation of polymer PFO on addition of multiwall carbon nanotubes
Malti Bansal, Ritu Srivastava, C. Lal, M. N. Kamalasanan and L. S. Tanwar, *Nanoscale*, 2010
DOI: 10.1039/c0nr00001a

Amino acid-assisted one-pot assembly of Au, Pt nanoparticles onto one-dimensional ZnO microrods
Xianghong Liu, Jun Zhang, Xianzhi Guo, Shihua Wu and Shurong Wang, *Nanoscale*, 2010
DOI: 10.1039/c0nr00015a

Luminescence resonance energy transfer from an upconverting nanoparticle to a fluorescent phycobiliprotein
Fiorenzo Vetrone, Rafik Naccache, Christopher G. Morgan and John A. Capobianco, *Nanoscale*, 2010
DOI: 10.1039/c0nr00126k

Doping single-walled carbon nanotubes through molecular charge-transfer: a theoretical study
Arun K. Manna and Swapan K. Pati, *Nanoscale*, 2010
DOI: 10.1039/c0nr00124d

Energy transfer study between Ce^{3+} and Tb^{3+} ions in doped and core-shell sodium yttrium fluoride nanocrystals
Pushpal Ghosh, Arik Kar and Amitava Patra, *Nanoscale*, 2010
DOI: 10.1039/c0nr00019a

Pt surface modification of SnO_2 nanorod arrays for CO and H_2 sensors
Hui Huang, C. Y. Ong, J. Guo, T. White, M. S. Tse and O. K. Tan, *Nanoscale*, 2010
DOI: 10.1039/c0nr00159g

Poly (acrylic acid)-capped lanthanide-doped BaFCl nanocrystals: synthesis and optical properties
Qiang Ju, Wenqin Luo, Yongsheng Liu, Haomiao Zhu, Renfu Li and Xueyuan Chen, *Nanoscale*, 2010
DOI: 10.1039/c0nr00116c

Enhanced Cu emission in ZnS : Cu,Cl/ZnS core–shell nanocrystals
Carley Corrado, Morgan Hawker, Grant Livingston, Scott Medling, Frank Bridges and Jin Z. Zhang, *Nanoscale*, 2010
DOI: 10.1039/c0nr00056f

Synthesis and characterization of zirconium-doped mesoporous nano-crystalline TiO_2
Kanattukara Vijayan Bineesh, Dong-Kyu Kim and Dae-Won Park, *Nanoscale*, 2010
DOI: 10.1039/c0nr00108b

Zn-doped nanocrystalline TiO_2 films for CdS quantum dot sensitized solar cells
Guang Zhu, Zujun Cheng, Tian Lv, Likun Pan, Qingfei Zhao and Zhuo Sun, *Nanoscale*, 2010
DOI: 10.1039/c0nr00087f

Effect of synergy on the visible light activity of B, N and Fe co-doped TiO_2 for the degradation of MO
Mingyang Xing, Yongmei Wu, Jinlong Zhang and Feng Chen, *Nanoscale*, 2010
DOI: 10.1039/c0nr00078g

Facile synthesis of lanthanide nanoparticles with paramagnetic, down- and up-conversion properties
Zhengquan Li and Yong Zhang, *Nanoscale*, 2010
DOI: 10.1039/c0nr00073f

Glucose oxidase-doped magnetic silica nanostrutures as labels for localized signal amplification of electrochemical immunosensors
Jingjing Ren, Dianping Tang, Biling Su, Juan Tang and Guonan Chen, *Nanoscale*, 2010
DOI: 10.1039/b9nr00416e

The role of ellipticity on the preferential binding site of Ce and La in C_{78}-D_{3h}—A density functional theory study
K. Muthukumar and J. A. Larsson, *Nanoscale*, 2010
DOI: 10.1039/c0nr00021c

Tuning the shape and thermoelectric property of PbTe nanocrystals by bismuth doping
Qian Zhang, Ting Sun, Feng Cao, Ming Li, Minghui Hong, Jikang Yuan, Qingyu Yan, Huey Hoon Hng, Nianqiang Wu and Xiaogang Liu, *Nanoscale*, 2010
DOI: 10.1039/c0nr00115e

Tuning the shape and thermoelectric property of PbTe nanocrystals by bismuth doping

Qian Zhang,[a] Ting Sun,[b] Feng Cao,[c] Ming Li,[d] Minghui Hong,[ef] Jikang Yuan,[c] Qingyu Yan,[b] Huey Hoon Hng,[b] Nianqiang Wu[d] and Xiaogang Liu*[a]

Received 13th February 2010, Accepted 15th March 2010
First published as an Advance Article on the web 19th May 2010
DOI: 10.1039/c0nr00115e

We report the synthesis of a series of monodispersed Bi-doped PbTe nanocrystals with tunable morphologies by using a doping precursor of bismuth(III) 2-ethylhexanoate. The as-synthesized $Pb_{1-x}Bi_xTe$ ($x = 0.005, 0.010, 0.015, 0.020$) nanocrystals are characterized by X-ray diffraction, X-ray photoelectron spectroscopy and Hall measurements. The nanocrystals with controlled spherical, cuboctahedral, and cubic shapes were readily prepared by varying the Bi doping concentration. Thermoelectric investigation of these nanocrystals shows that the Bi^{3+} doping increases electrical conductivity from 350 to 650 K and changes the Seebeck coefficient sign from positive to negative.

Introduction

Thermoelectric (TE) materials can directly convert thermal energy into electrical energy upon applying a thermal gradient to the materials. These materials are playing an increasingly important part in a diverse range of applications as heat pumps and electrical power generators.[1–4] The efficiency of TE materials can be measured by the material's dimensionless figure of merit ZT ($ZT = \alpha^2\sigma T/\kappa$, where α is the Seebeck coefficient or thermopower, T is the absolute temperature, and σ and κ are the electrical conductivity and thermal conductivity). The thermal conductivity comprises contribution from electrons and phonons.[5]

Maximizing ZT is often achieved by minimizing the thermal conductivity by promoting interface-phonon scattering. It has been proposed that nanostructured materials can enhance ZT due to the occurrence of the quantum confinement effect, which increases thermopower α resulting from an increased local density of states near the Fermi level.[6–8] Despite recent development in nanocrystal synthesis,[9–17] it has been challenging to prepare small-sized thermoelectric nanocrystals with controlled doping composition and concentration.[18–20] For instance, although bismuth (Bi) has been used as an n-type dopant in PbTe thin films and bulk materials for thermoelectric studies,[21,22] the preparation of well-defined Bi-doped PbTe nanoparticles with controlled doping levels remains a substantial challenge.

In this study, we show that it is plausible to synthesize monodispersed Bi-doped PbTe nanocrystals with controlled sizes and morphologies by utilizing bismuth(III) 2-ethylhexanoate as the Bi precursor. Importantly, we show that the Bi doping results in electrical conductivity enhancement in the PbTe nanocrystals, providing promising uses for thermoelectric applications.

Experimental

In a typical synthesis, 1 mmol of lead acetate trihydrate (> 99%) and stoichiometric amounts of bismuth(III) 2-ethylhexanoate were dissolved in 5 ml of 1-octadecene and 1 ml of oleic acid (both technical grade, 90%) in a 50 ml flask. The resulting mixture was heated at 90 °C under stirring for three hours to form a light yellow solution. A stock solution (0.75 M) of tellurium was separately prepared by adding the tellurium powder (99.8%) into trioctylphosphine (≥ 97%) with vigorous stirring overnight. Subsequently, a 4 ml tellurium stock solution was quickly injected into the solution of lead acetate at a temperature of 150 °C. After two minutes, the flask was cooled in an ice bath to precipitate the nanocrystals. The as-formed nanocrystals were washed with absolute ethanol several times, further precipitated by centrifugation, and re-dispersed with cyclohexane. All syntheses were performed in an argon atmosphere using a Schlenk line.

X-Ray power diffraction (XRD) analysis was carried out on a Siemens D5005 X-ray diffractometer with Cu Kα radiation ($\lambda = 1.5406$ Å). The particle morphology and selected area electron diffraction (SAED) were examined by transmission electron microscopy (TEM, JEOL 2010) operating at an acceleration voltage of 200 kV. X-Ray photoelectron spectra (XPS) were performed with a PHI 5000 Versa Probe system (Physical Electronics, MN) using a monochromatic Al Kα X-ray source (1486.6 eV). The pass energy of the hemisphere analyzer was maintained at 117.4 eV for survey scan and 58.7 eV for high-resolution scan, while the takeoff angle was fixed at 45°. Binding energies of XPS spectra were corrected by referencing the C1s signal of adventitious hydrocarbon to 284.8 eV. XPS data fittings were carried out with PHI multipak™ software using the

[a]*Department of Chemistry, National University of Singapore, Singapore, 117543. E-mail: chmlx@nus.edu.sg; Fax: +65-65161791*
[b]*Department of Materials Science and Engineering, Nanyang Technological University, Singapore, 639798*
[c]*Department of Applied Physics, The Hong Kong Polytechnic University, Kowloon, Hong Kong SAR, China*
[d]*Department of Mechanical and Aerospace Engineering, West Virginia University, Morganton, USA 26506*
[e]*Department of Electrical and Computer Engineering, National University of Singapore, Singapore, 117543*
[f]*Optical Materials and Systems Division, Data Storage Institute, A*STAR, Singapore, 117608*

Gauss-Lorenz mode and Shirley background. For preparation of nanoparticle films, the as-synthesized nanoparticles were washed with $N_2H_4 \cdot H_2O$ and ethanol (v/v; 1 : 4) to remove capping surfactants and re-dispersed in ethanol prior to spray-coating onto a glass substrate and subsequently annealing under H_2/Ar at 350 °C for 30 min. The electrical properties of the films were measured by a ZEM-3 Seebeck meter from 350 to 650 K. The thickness of the film was obtained by using a surface profile scanning system (α-step IQ). The surface morphology of the films was investigated by field-emission scanning electron microcopy (SEM, JEOL6710). The Hall measurements were conducted on a Lake Shore 7600 Hall measurement system from 300 K to 100 K.

Results and discussion

The crystal structures of the as-synthesized Bi-doped PbTe ($Pb_{1-x}Bi_xTe$; $x = 0$, 0.005, 0.010, 0.015 and 0.020) samples were first examined by XRD and the results are shown in Fig. 1. All diffraction peaks can be indexed to face-centered cubic (fcc) rock-salt structures with a space group of *Fm*3*m* (JCPDS: 78-1904). The slight peak shifts towards higher diffraction angles in the X-ray powder diffraction patterns as a function of the Bi^{3+} ion concentration, can be attributed to the contraction in unit-cell volume due to the substitution of Pb^{2+} ions by smaller Bi^{3+} ions in the host lattice. The lattice parameter was found to decrease with an increase in the dopant concentration (Fig. 1, inset). The solubility limit of bismuth in PbTe was estimated to be $x = 0.015$.

It has been reported that lead chalcogenide nanoparticles with controlled feature size and morphology can be obtained by varying the reaction time, surfactant concentration, and ratio of metal precursors.[23,24] We found that the doping of Bi^{3+} at different doping levels through use of bismuth(III) 2-ethylhexanoate as the doping precursor resulted in the formation of PbTe nanoparticles with tunable particle size (10–15 nm) and morphology. To exclude the possibility of reaction time effect on the nanocrystal growth, all the reactions were carried out for two minutes and immediately quenched by pouring the reaction mixtures into an ice bath. The effect of Bi^{3+} doping on the morphology of the nanocrystals was presented in Fig. 2. With no Bi^{3+} added, monodispersed spherical PbTe nanoparticles were obtained with an average particle size of 10 nm.[25] On doping of Bi^{3+} with increased concentrations ($x = 0.005$, 0.010, 0.015), the nanocrystal morphology changes from spherical shape to cuboctahedral and cubic shapes. Notably, the doping of Bi^{3+} also leads to an increase in the nanocrystal size.

The shape evolution of the PbTe nanocrystals as a function of Bi^{3+} dopant can be attributed to the relative growth rates on different crystallographic planes.[26,27] In the rock-salt crystal structure, the {111} plane generally has a higher surface energy than the {100} plane.[23] On increasing reaction time, the {111} facets grow faster than the {100} facets, resulting in the formation of cubic-shaped nanocrystals dominated with {100} planes. For example, it was reported that the spherical/cuboctahedral-to-cubic shape conversion for pure PbTe nanocrystals requires more than 20 min of reaction time.[24] In contrast, our doping approach results in the shape conversion within 2 min. The effect on shortening the reaction time can be ascribed to the addition of 2-ethylhexanoate, which stabilizes the {100} facets and promotes the relative growth rate of the {111} facets.

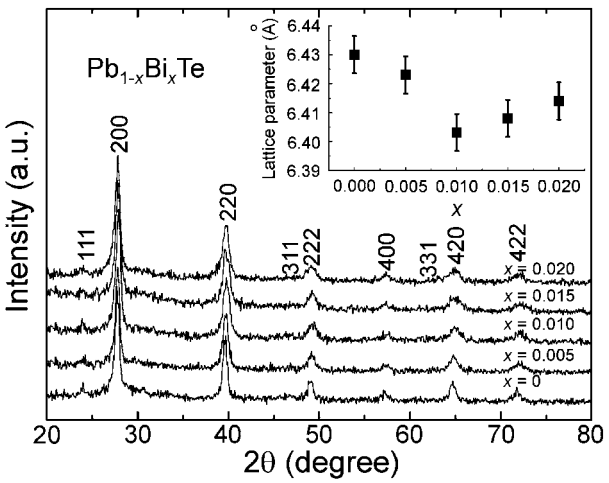

Fig. 1 XRD patterns of the as-synthesized $Pb_{1-x}Bi_xTe$ ($x = 0$, 0.005, 0.010, 0.015 and 0.020) samples (inset: the lattice parameter of the samples as a function of Bi^{3+} doping concentration x).

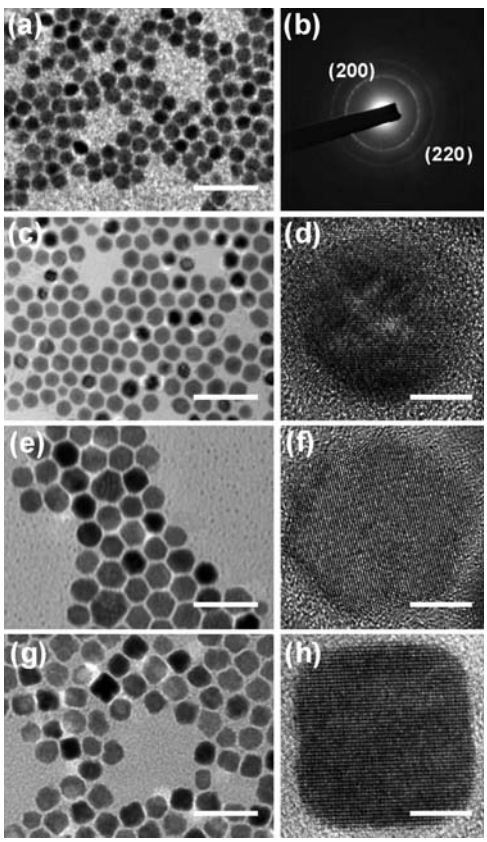

Fig. 2 (a), (c), (e) and (g) Corresponding TEM images of the as-synthesized $Pb_{1-x}Bi_xTe$ nanocrystals at $x = 0$, 0.005, 0.010 and 0.015, respectively. (b) SAED pattern obtained for samples shown in Fig. 2(a), indicating cubic PbTe structures. (d), (f) and (h) Corresponding HRTEM images of the nanocrystals shown in (c), (e) and (g), respectively. The scale bars are 50 nm for (a), (c), (e) and (g) and are 5 nm for (d), (f) and (h).

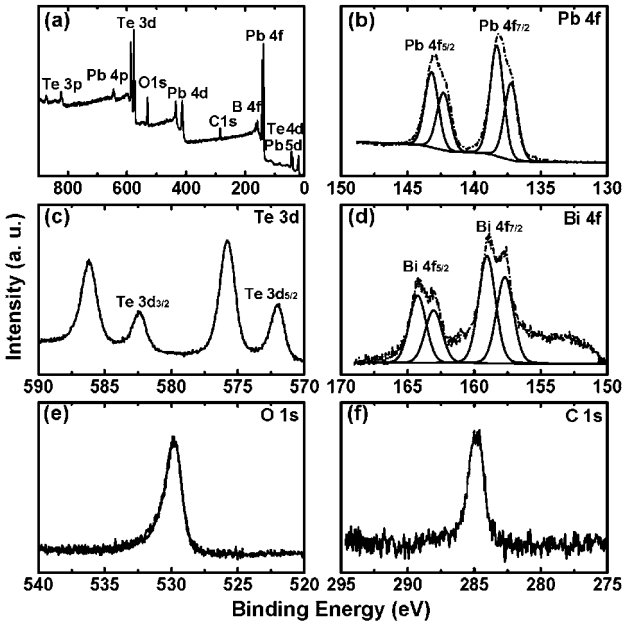

Fig. 3 (a) XPS survey scan of the as-synthesized $Pb_{0.99}Bi_{0.01}Te$ nanoparticles. (b)–(f) High-resolution XPS spectra of respective Pb4f, Te3d, Bi4f, O1s and C1s regions of the $Pb_{0.99}Bi_{0.01}Te$ nanoparticles.

To verify the crystal composition and the presence of stabilizing molecules bound to the crystal surface, the PbTe nanocrystals doped with 1 mol% Bi^{3+} were examined by XPS as shown in Fig. 3. Fig. 3(a) shows the XPS spectrum that provides a survey scan of the nanocrystals. All peaks can be assigned to Pb, Te, Bi, O and C. The $Pb4f_{7/2}$ and $Pb4f_{5/2}$ peaks were observed at 137.2 and 142.3 eV respectively, which were the characteristic values for PbTe (Fig. 3(b)). The high-binding-energy shoulder peaks at 138.4 and 143.2 eV correspond to the expected chemical shifts for either $Pb(OH)_2$ or PbO (Fig. 3(b)).[28] The $Te3d_{5/2}$ and $Te3d_{3/2}$ peaks were observed at 571.9 and 582.3 eV, which were diagnostic of PbTe (Fig. 3(c)). Two groups of peaks at 575.8 and 586.2 eV were assigned to TeO_2 (Fig. 3(c)).[28] The two sub-bands of Bi4f at 158 ($Bi4f_{5/2}$) and 163.4 eV ($Bi4f_{7/2}$) further confirm the presence of Bi^{3+} dopant in PbTe nanocrystals.[29] The high-binding-energy shoulder peaks at 159 and 164.4 eV were assigned to Bi_2O_3 (Fig. 3(d)). The C1s and O1s peaks at 284.8 and 530 eV were attributed to oleic acid or 2-ethylhexanoate molecules bound to the particle surface (Fig. 3(e) and (f)).

To evaluate the TE application of the Bi-doped nanoparticles, the nanoparticle thin films doped with varied amounts of Bi were prepared by an air brush spray system. The hydrazine treatment was employed to remove the organic ligands for increased electrical contact of the nanoparticle systems.[30] The surface morphology of an as-prepared film after annealing at 350 °C is shown in Fig. 4(a). Upon annealing, the nanoparticles were enlarged to 20–30 nm. The quantum confinement effect is expected as the average size of the enlarged nanoparticles is still smaller than the Bohr exciton radius (~46 nm) of PbTe.[31] The electrical resistance and the Seebeck coefficient of the samples were measured from 350 to 650 K and plotted as a function of temperature in Fig. 4(b) and (c), respectively. In contrast to the PbTe nanoparticle film without the Bi^{3+} dopant, the films made

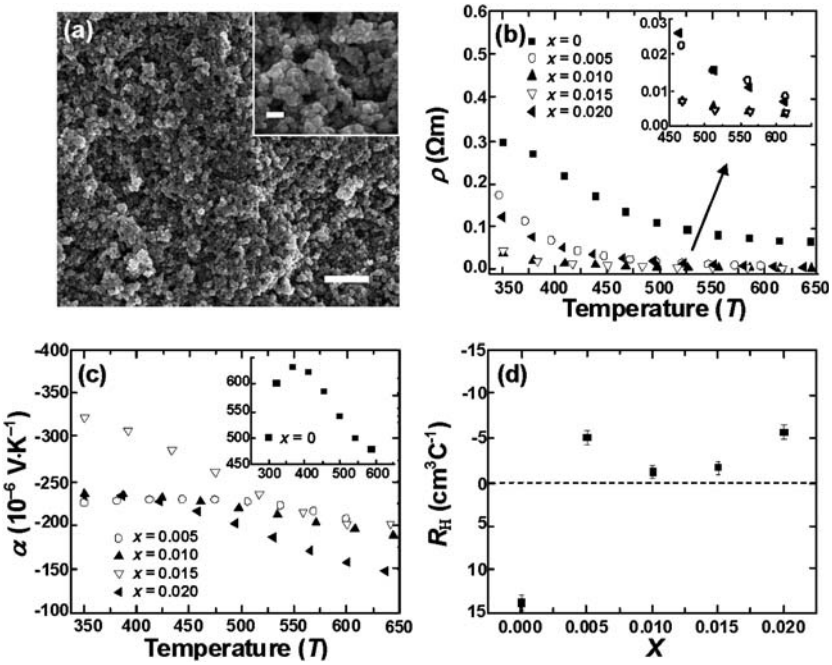

Fig. 4 (a) A representative SEM image of the film made from Bi-doped PbTe nanoparticles. The scale bar is 1 μm. Inset is a high magnification SEM of the film shown in Fig. 4(a) and the scale bar is 100 nm. (b) Temperature dependence studies of the electrical resistance for the films made from $Pb_{1-x}Bi_xTe$ ($x = 0$, 0.005, 0.010, 0.015, 0.020) nanoparticles. Inset is an enlarged area of electrical resistance measured between 450 and 650 K. (c) Corresponding Seebeck coefficient measurements obtained from the films made from Bi-doped PbTe nanoparticles (inset: the Seebeck coefficient measurement of the film made from undoped PbTe nanoparticles). (d) Corresponding Hall coefficient measurements obtained from the films made from Bi-doped and undoped PbTe nanoparticles.

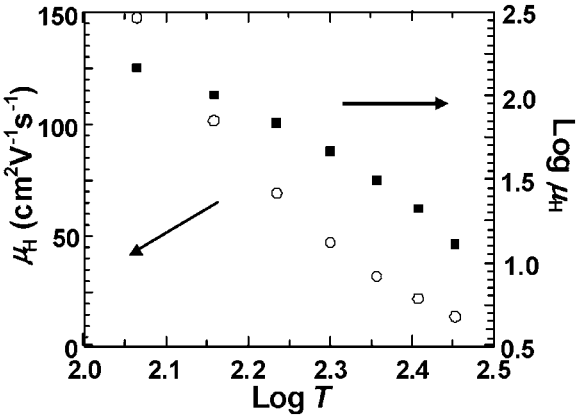

Fig. 5 μ_H (left panel) and logμ_H (right panel) as a function of log$T$ for the $Pb_{0.99}Bi_{0.01}Te$ nanoparticle film.

from Bi-doped PbTe nanocrystals showed marked decreases of electrical resistance (Fig. 4(b)) and negative Seebeck coefficients (Fig. 4(c)). The negative Seebeck coefficients, which are consistent with the results obtained by the Hall measurements shown in Fig. 4(d), provide another proof of the successful doping of the Bi^{3+} into the PbTe nanocrystals. The Bi-doped PbTe nanocrystals doped with 1.5 mol% Bi^{3+} exhibited a high Seebeck coefficient of -325 μV K^{-1} at 350 K, which is consistent with the theoretical value (-350 μV K^{-1}) for n-type PbTe structures that possess the same electron carrier concentration.[31]

The Hall mobility of films made from Bi-doped PbTe nanocrystals (1 mol% Bi^{3+}) was derived by using $\mu_H = R_H/\rho$, (where μ_H, R_H, and ρ refer to the Hall mobility, Hall coefficient and the electrical resistance, respectively) and plotted as a function of log$T$ from 300 to 100 K (Fig. 5, left panel). The Hall mobility of the Bi-doped film (~0.6 cm^2 V^{-1} s^{-1}) at 300 K is lower than that of the undoped film (~2.1 cm^2 V^{-1} s^{-1}), which is attributed to the inverse relationship between carrier concentration and Hall mobility. In the right panel of Fig. 5, the log μ_H *vs.* log$T$ graph was presented, giving rise to the power exponent δ ($\mu \approx T^{-\delta}$) of ~1.9 at 100–200 K and ~3.5 at 200–300 K with the logμ_H curve deviating from a straight line at ~200 K. The results, which are also found in $Pb_{0.99}La_{0.01}Te$ bulk materials, are consistent with the behavior of the weakly or intermediate degenerate n-type PbTe semiconductors.[32]

Conclusions

We have developed a new method for the synthesis of single-crystalline Bi-doped PbTe nanocrystals by using bismuth(III) 2-ethylhexanoate as the Bi^{3+} precursor. The incorporation of the Bi^{3+} dopant at different doping levels in the nanocrystal host lattice was confirmed by XRD, XPS, and Hall measurements. Importantly, we have demonstrated that the doping approach imparts a substantial impact on the growth process to give dual control over the size and shape of the resulting nanocrystals. Investigation of the thermoelectric properties of films made from these nanocrystals shows decreased electrical resistance from 350 to 650 K as compared to undoped nanocrystal films.

Acknowledgements

This work was supported in part by the National University of Singapore (NUS) Academic Research Fund, the Singapore-MIT Alliance, and the Agency for Science, Technology and Research (A*STAR). X. L. is grateful to the NUS for a Young Investigator Award. We thank L. Tian and J. Xu for technical assistance.

Notes and references

1 B. C. Sales, *Science*, 2002, **295**, 1248.
2 F. Zhou, J. Szczech, M. T. Pettes, A. L. Moore, S. Jin and L. Shi, *Nano Lett.*, 2007, **7**, 1649.
3 W. Zhou, J. Zhu, D. Li, H. H. Hng, F. Y. C. Boey, J. Ma, H. Zhang and Q. Yan, *Adv. Mater.*, 2009, **21**, 3196.
4 T. M. Tritt, *Science*, 1996, **272**, 1276.
5 *Thermoelectrics Handbook: Macro to Nano*, ed. D. M. Rowe, Taylor & Francis, New York, 2006.
6 M. S. Dresselhaus, G. Chen, M. Y. Tang, R. Yang, H. Lee, D. Wang, Z. Ren, J. Fleurial and P. Gogna, *Adv. Mater.*, 2007, **19**, 1043.
7 J. P. Heremans, V. Jovovic, E. S. Toberer, A. Saramat, K. Kurosaki, A. Charoenphakdee, S. Yamanaka and G. J. Snyder, *Science*, 2008, **321**, 554.
8 B. Poudel, Q. Hao, Y. Ma, Y. Lan, A. Minnich, B. Yu, X. Yan, D. Wang, A. Muto, D. Vashaee, X. Chen, J. Liu, M. S. Dresselhaus, G. Chen and Z. Ren, *Science*, 2008, **320**, 634.
9 Y. Wu, C. Wadia, W. Ma, B. Sadtler and A. P. Alivisatos, *Nano Lett.*, 2008, **8**, 2551.
10 M. Oh and C. A. Mirkin, *Nature*, 2005, **438**, 651.
11 X. Liu, *Angew. Chem., Int. Ed.*, 2009, **48**, 3018.
12 R. S. Selinsky, D. J. Keavney, M. J. Bierman and S. Jin, *Appl. Phys. Lett.*, 2009, **95**, 202501.
13 Q. Yan, H. Chen, W. Zhou, H. H. Hng, F. Y. C. Boey and J. Ma, *Chem. Mater.*, 2008, **20**, 6298.
14 F. Wang, Y. Han, C. S. Lim, Y. Lu, J. Wang, J. Xu, H. Chen, C. Zhang, M. Hong and X. Liu, *Nature*, 2010, **463**, 1061.
15 F. Wang and X. Liu, *Chem. Soc. Rev.*, 2009, **38**, 976.
16 L. Cademartiri, J. Bertolotti, R. Sapienza, D. S. Wiersma, G. Von Freymann and G. A. Ozin, *J. Phys. Chem. B*, 2006, **110**, 671.
17 F. Wang, X. Xue and X. Liu, *Angew. Chem., Int. Ed.*, 2008, **47**, 906.
18 G. M. Dalpian and J. R. Chelikowsky, *Phys. Rev. Lett.*, 2006, **96**, 226802.
19 S. C. Erwin, L. Zu, M. I. Haftel, A. L. Efros, T. A. Kennedy and D. J. Norris, *Nature*, 2005, **436**, 91.
20 T. Ji, W. Jian and J. Fang, *J. Am. Chem. Soc.*, 2003, **125**, 8448.
21 T. C. Harman, M. P. Walsh, B. E. Laforge and G. W. Turner, *J. Electron. Mater.*, 2005, **34**, L19.
22 Y. Chen, T. J. Zhu, S. H. Yang, C. Yu and X. B. Zhao, *J. Phys. D: Appl. Phys.*, 2010, **43**, 035405.
23 S. M. Lee, S. N. Cho and J. Cheon, *Adv. Mater.*, 2003, **15**, 441.
24 W. Lu, J. Fang, K. L. Stokes and J. Lin, *J. Am. Chem. Soc.*, 2004, **126**, 11798.
25 J. E. Murphy, M. C. Beard, A. G. Norman, S. P. Ahrenkiel, J. C. Johnson, P. Yu, O. I. Micic, R. J. Ellingson and A. J. Nozik, *J. Am. Chem. Soc.*, 2006, **128**, 3241.
26 Z. L. Wang, *J. Phys. Chem. B*, 2000, **104**, 1153.
27 X. Liu, N. Wu, B. H. Wunsch, R. J. Barsotti Jr. and F. Stellacci, *Small*, 2006, **2**, 1046.
28 Y. Yang, S. C. Kung, D. K. Taggart, C. Xiang, F. Yang, M. A. Brown, A. G. Guell, T. J. Kruse, J. C. Hemminger and R. M. Penner, *Nano Lett.*, 2008, **8**, 2447.
29 E. J. Menke, M. A. Brown, Q. Li, J. C. Hemminger and R. M. Penner, *Langmuir*, 2006, **22**, 10564.
30 D. V. Talapin and C. B. Murray, *Science*, 2005, **310**, 86–90.
31 T. J. Zhu, X. Chen, Y. Q. Cao and X. B. Zhao, *J. Phys. Chem. C*, 2009, **113**, 8085.
32 K. Ahn, C. P. Li, C. Uher and M. G. Kanatzidis, *Chem. Mater.*, 2009, **21**, 1361.